COURSE 1

ACCRETION SIGNATURES IN YOUNG STELLAR OBJECTS

NURIA CALVET

Smithsonian Astrophysical Observatory, Cambridge, USA

PHOTO: height 7.5cm, width 11cm

Contents

ACCRETION SIGNATURES IN YOUNG STELLAR OBJECTS

Nuria Calvet

Abstract

Mass accretion onto the star is taken place in young stellar objects, providing the energy needed to power the excess emission observed at all wavelength bands. Signatures that allow us to identify and quantify accretion processes are reviewed in these lectures.

1 Introduction

In the process of star formation, matter is transfered from molecular clouds to stars. This accretion of matter leaves distinctive signatures, for instance, redshifted absorptions in spectral lines indicating that matter is falling in. In addition, some energy losses observed in young stellar objects (YSO) need to be compensated by external sources. Gravitational potential energy is the best candidate to supply this need. Present models based on this hypothesis can consistently explain most of the emission properties of YSO. We will review the evidence in these lectures.

2 YSO

Samples of visible YSO are located in the HR diagram in Fig. 1, superimposed to the theoretical isochrones of [1]. The well known T Tauri stars (TTS) in the Taurus cloud have typical masses of a few tenths of $M_\odot$ [2]. However, the type extends to masses $\sim$ 2 - 3 $M_\odot$, in the high mass side, to objects in the sub-stellar limits, the brown dwarfs [3]. The Herbig Ae/Be stars (HAeBe) have masses $> 1.5 M_\odot$ [4]. Typical ages are $\sim$ 1 - 10 Myr.

The emerging flux of the visible YSO is characterized by excesses over photospheric fluxes appearing in emission lines and continua (see [5] for complete list of references). The emission lines show a wide range of conditions of formation. The forbidden lines indicate densities of $n_H \sim 10^5 cm^{-3}$ while the permitted lines require densities of up to $n_H \sim 10^{13} cm^{-3}$. Forbidden and optical/infrared (IR) permitted lines indicate temperatures in the

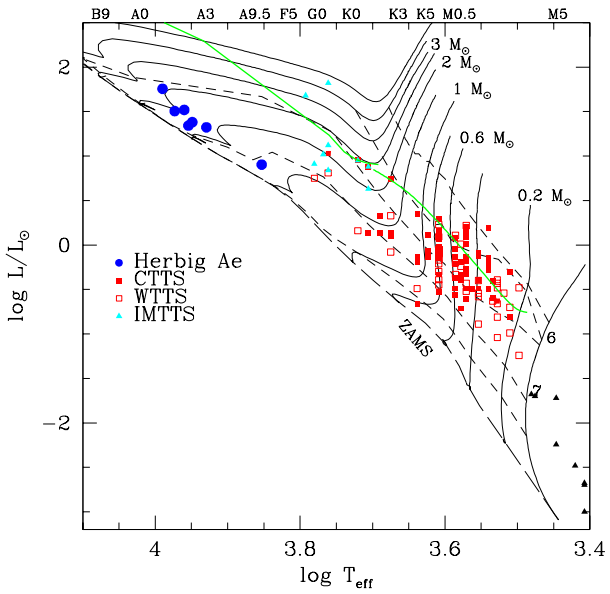

Fig. 1. HR diagram showing the location of visible YSO: Herbig Ae/Be stars, Classical T Tauri stars, Weak T Tauri stars, and intermediate mass T Tauri stars. The luminosity refers to the purely stellar luminosity. Evolutionary tracks for masses between 0.1 and 4 $\dot{M}$ (light solid lines) and isochrones between log t = 5.5 and 8 (dashed lines) are indicated. The heavy solid line is the birthline.

formation region of $T \sim 10^4$K, while lines of highly ionized species seen in the ultraviolet (UV) indicate $T \sim 10^{5-6}$K. Typical velocities range from $\sim$ 0 to a few hundred km s^{-1}. The continuum excess appears in the optical as a flux veiling the photospheric absorption lines, and in fluxes orders of magnitude higher than expected photospheric fluxes in the UV, IR, millimeter (mm) and radio emission.

TTS can be classified en two types: Classical T Tauri stars (CTTS) and weak T Tauri stars (WTTS). Initially, the classification was based on the equivalent width of Hα, with EW(Hα) < 10Å in WTTS [6]. It was soon recognized that the classification represented clear physical differences. CTTS have large IR excesses, which the WTTS lack. While WTTS have emission lines, these lines are not only generally weaker but much *narrower* than

CTTS. WTTS show no indication of veiling in their absorption lines, while CTTS show a wide range of veiling that correlates with near IR colors. Similarly, WTTS show *no* forbidden emission lines, while these lines are always present in CTTS [7]. The strength of the UV lines in WTTS, although higher or comparable to other type of very active stars, are order of magnitude lower than in CTTS [8]. The X-ray luminosity, on the other hand, appears to be similar in both types [9].

The total luminosity of a given TTS, including the excess emission if present, can be compared to the purely stellar luminosity, that is, the luminosity the stellar photosphere would have by itself. This can be estimated from the J band magnitude, where the contribution of the excess flux seem to be minimal ([2], see however, measurements of veiling at J by [10])). The observed luminosity of the WTTS agrees with the stellar luminosity. In contrast, the CTTS show luminosities in average 10% higher, and in some cases much higher than that due to the star alone ([5], Fig.6.3). *An additional source of energy is required to compensate for this extra energy.* The most likely source is accretion energy, that is *gravitational potential energy* ([11]). This source must also be responsible for other peculiarities that stars with excess energy show, namely, the broad emission lines, the veiling, the IR excess, and the forbidden line emission. In the next sections, we will review models of mass accretion for the CTTS which can account for these properties.

TTS share properties with other active stars in the HR diagram. Strong magnetic fields, of the order of a few KG, have been detected in both types of TTS, by measuring the Zeeman splitting in magnetic sensitive absorption lines [12, 13]). Similar magnetic field strengths are indicated by circular spectropolarimetry of emission lines [14]. These magnetic fields will induce surface activity as it does in other active stars. The general level of activity observed in WTTS, comparable or higher than active stars of other types, can be explained by these type of phenomena. The generally high rotational velocities observed in WTTS would support this hypothesis [15, 16], but cannot explain the energy output of the CTTS, which are rotating more slowly.

Some YSO are also found embedded in molecular clouds, so heavily extincted that only appear in the infrared and beyond. The characteristics of these objects can be understood if they are *protostars*, that is, they are still actively receiving mass from the cloud. Besides the close association with the densest cores, direct evidence of infall motions in molecular line profiles has been obtained ([17, 18]). These objects are also called Class I, in which the flux increases with wavelength in the near-mid infrared. In contrast, the slope is negative in the visible objects, classified as Class II. [19]. Typical ages for these objects can be estimated from the relative numbers of embedded and visible objects in a given cloud. For Taurus,

there are $\sim$ 10 times as many visible stars as protostars. With a typical age of 1-2 Myr for the visible TTS, the protostellar phase is $\sim$ 0.1 - 0.2 Myr.

It is difficult to asses the *stellar* properties of protostars, since they are so embedded. We can estimate the luminosities of the objects by measuring the total energy emitted in the infrared; this energy has been absorbed by the dust in the circumstellar material and re-radiated at longer wavelengths. However, this luminosity can be either stellar luminosity, that is, due to the release of thermal energy as the star contracts, or energy released as matter is accreted onto the star. As we will see later, present evidence indicates that the observed luminosity corresponds to stellar luminosity for most protostars.

3 Formation mechanisms

Accretion energy is the most likely source for the extra emission observed in YSO, and it is naturally expected to be released in the process of star formation. Stars are formed by gravitational contraction of cores, the densest part of molecules clouds. Observations indicate that these cores are slowly rotating [20]. Collapse under conservation of energy and angular momentum results in the formation of a disk [21], [22]. The material with the highest angular is that at larger radius, where most of the mass of the core is for reasonable density laws. This means that most of the mass of the core lands on the disk, since it has too much angular momentum to go directly to the star. Thus, accretion occurs schematically in two stages: cloud to disk, and disk to star, which we refer to in these lectures as *infall* and *accretion* proper, respectively.

Relevant luminosities in these processes are the potential energy released in the (radial) infall to the star, L_{inf}(star), the energy released in the infall to the disk, L_{inf}(disk), the accretion luminosity released as matter is accreted from the disk onto the star, L_{acc}, the stellar luminosity, L_*, and the observed luminosity L_{obs}. We will estimate and compare these luminosities next.

The infall luminosities can be estimated by $L_{inf} \sim G\,\dot{M}_{inf} M_*/R$, where $\dot{M}_{inf}$ is the infall mass accretion rate, M_* is the stellar mass and R is the radius where material lands. R is equal to the stellar radius R_* for infall to the star and to the disk radius for infall to the disk. Objects in this phase are expected to be on the *birthline*, that is, the locus in the HR diagram of objects which are accreting mass [23, 24]. Birthline calculations yield an estimate of $M_*/R_* \sim 0.5$, and $R_* \sim 2\mathrm{R}_\odot$ [23, 24], while disk radii are of the order of 10 - 100 AU.

The mass infall rate can be estimated from the density of the infalling envelope model that produces a spectral energy distribution (SED) similar to that observed, since by mass conservation $\dot{M}_{inf} \sim 4\pi r^2 \rho v$, assuming spher-

ical infall at large distances, with v the free-fall velocity, $v = (GM_*/r)^{1/2}$. Radiative transfer calculations for infalling envelope models have been carried out for Class I objects in the Taurus cloud [25], yielding an average $\dot{M}_{inf} \sim 4 \times 10^{-6} M_\odot yr^{-1}$.

With this mass infall rate, $L_{inf}(\mathrm{star}) \sim 15 - 30 \mathrm{L}_\odot$, higher than the observed luminosities, $L_{obs} \leq 1\,\mathrm{L}_\odot$. This has been named the "luminosity problem" [26], but actually is not a problem. For typical disk radii, $L_{inf}(\mathrm{disk}) \sim 0.002 - 0.03 \mathrm{L}_\odot$, so if infall occurs onto the disk, as expected from angular momentum conservation, then the infall luminosities are much lower than the observed luminosities.

The stellar luminosity can be estimated from the birthline, see Fig. 1. It can be seen that for low mass objects and typical mass infall rates, protostars luminosities are expected to be of the same order of magnitude as visible objects. In fact, in the Taurus cloud, the observed distribution of luminosities of protostars and visible stars are similar, which seems to suggest that the luminosities of protostars are actually stellar luminosities.

It still remains to quantify the accretion luminosity, that is, the energy released in the transfer of matter from the disk onto the star, to completely identify the source of luminosity in Class I objects, and thus determine if the luminosity is an accretion signature in these objects.

4 Accretion luminosity and mass accretion rate

Disk emission in protostars tends to be hidden by the absorption and emission of the infalling envelope, which has sizes $\sim$ thousands of AU, surrounding the star and the 10 - 100 AU disk. The best determination of the accretion luminosity can be obtained in the visible objects, in which the envelope has already dissipated.

In CTTS, the excess flux veiling the absorption lines in the optical and dominating in the UV can be extracted by subtraction of the photospheric fluxes. The luminosity in this excess flux, if identified with accretion energy, gives an estimate of the accretion luminosity. With M_* and R_* from the position in the HR diagram of a given star, the accretion luminosity $L_{acc} = G\dot{M}M_*/R_*$ yields the mass accretion rate $\dot{M}$. Fig. 2 shows the mass accretion rate measurements for CTTS in Taurus and Chameleon [27, 28]. The mean accretion luminosity for CTTS in these clouds is $\sim 0.1 \mathrm{L}_\odot$, and the corresponding mean mass accretion rate is $10^{-8} M_\odot yr^{-1}$.

5 Magnetospheric accretion

We can now begin to identify the mechanisms by means of which accretion onto the star takes place. The star is surrounded by a disk through which mass is flowing onto the star at a rate $\dot{M}$. The star, in turn, has a magnetic

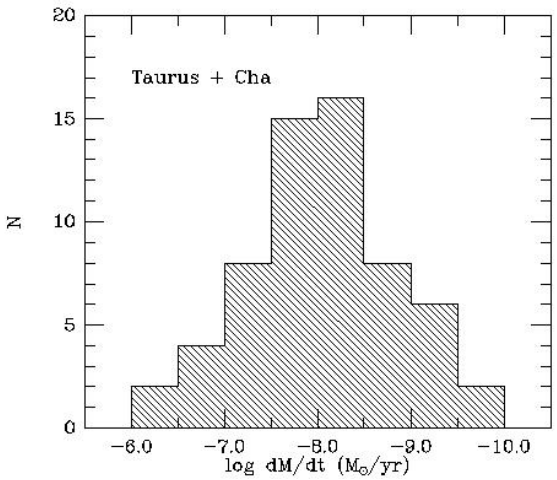

Fig. 2. Distribution of mass accretion rates for CTTS in the associations of Taurus and Chameleon [28]

field of a few KG at its surface. For spherical accretion, and in the case of a dipolar magnetic field, accretion is halted by the magnetic field at a radius

$$r_t = 7R_* \left(\frac{B}{1KG}\right)^{4/7} \left(\frac{\dot{M}}{10^{-8} M_\odot yr^{-1}}\right)^{-2/7} \left(\frac{M_*}{0.5\mathrm{M}_\odot}\right)^{-1/7} \left(\frac{R_*}{2\mathrm{R}_\odot}\right)^{5/7} \tag{5.1}$$

[29]. For disk accretion, $R_t \sim \gamma r_t$, with $\gamma < 1$, 1/3 - 2/3 [30–32]. So, for the typical parameters characterizing CTTS (see Fig. 1) , the inner disk is truncated at a few stellar radii by the stellar magnetic field. Matter falls onto the star along field lines with essentially the free-fall velocity (the thermal pressure is expected to be much smaller than the ram pressure).

Before the role of magnetic fields was recognized, disks were expected to join the star through a boundary layer. In this layer, material in the innermost disk annulus, rotating at the Keplerian rotation at the stellar surface, $v_K \sim 217(M_*/0.5\mathrm{M}_\odot)^{1/2}(\mathrm{R}_*/2\mathrm{R}_\odot)^{-1/2}\mathrm{km\,s^{-1}}$, would slow down to the low surface rotational velocities observed, $< 15\mathrm{km\,s^{-1}}$. Magnetospheric accretion, in addition to being consistent with the measured values of magnetic fields and mass accretion rates, implies a much larger emitting volume and larger infall velocities than the boundary layer model; both properties predict emission indicators in much better agreement with observations.

Magnetospheric accretion has several important predictions which can be compared to the observations. Lines formed in the magnetospheric flow have characteristic profiles; in addition, matter joins the star through an

accretion shock formed at the stellar surface, which also produces characteristic emission. We review them in turn.

5.1 Line formation in the magnetospheric flow

The emission profiles of permitted lines in CTTS are characterized by peaks at nearly zero velocities, slightly blueshifted in a few cases. Superimposed to the emission, they show a blue-shifted absorption component and in some cases a *red-shifted* absorption component (cf. [34]). These profiles cannot be due to a stellar wind, which produces the typical P-Cygni profile, with a peak red-shifted to velocities of the order of the terminal velocity, a few hundred $\mathrm{km\,s^{-1}}$, and a blue-shifted absorption component that goes below the continuum [35]. They cannot be produced in a boundary layer wind either, because profiles would be too broadened by the rotation of the emitting region [36]. In contrast, the maximum contribution to the lines in magnetospheric infall comes from the region where matter is getting lifted from the disk, which has the largest volume; the velocity of the matter in this region is nearly zero. The wings, on the other hand, are formed where the flow approaches the stellar surface, resulting in a line width comparable to the free-fall velocity at the stellar surface. In addition, if the line of sight intersects the infalling material in front of the accretion shock, which is emitting as we will see, at much higher temperatures than the stellar photosphere, a red-shifted absorption component is formed (Fig. 3). Thus, magnetospheric infall can naturally explain the main features of observed emission line profiles in CTTS.

Detailed calculations for dipolar fields and axially-symmetric flows have confirmed these expectations for CTTS [37]. Observed line profiles of H and Na lines have been calculated, producing excellent agreement with observations of CTTS covering the observed range of mass accretion rate [37]. The wind only has a major contribution to the Hα emission in stars with the highest $\dot{M}$, in agreement with the characteristic P Cygni profiles of these lines. But even in these stars, lines with lower opacity like the Paschen and Bracket lines or the Na lines, show typical magnetospheric profiles [37]. Therefore, *broad, nearly centered profiles in emission lines of low mass TTS represent one of the most important accretion signatures.* The presence of red-shifted absorption components, of course, reinforces the interpretation of accretion.

Magnetospheric accretion has also been identified in HAeBe. In this case, however, the typical magnetospheric profile is characterized by a broad central or slightly red-shifted absorption. In contrast to CTTS, where the infalling material can only absorb radiation from the accretion shock, in HAeBe, the flow can absorb radiation from the much hotter stellar disk, giving rise to the broad absorption. As illustration, Balmer line profiles of the HAeBe star UX Ori are shown in Fig. 4, compared to the predictions

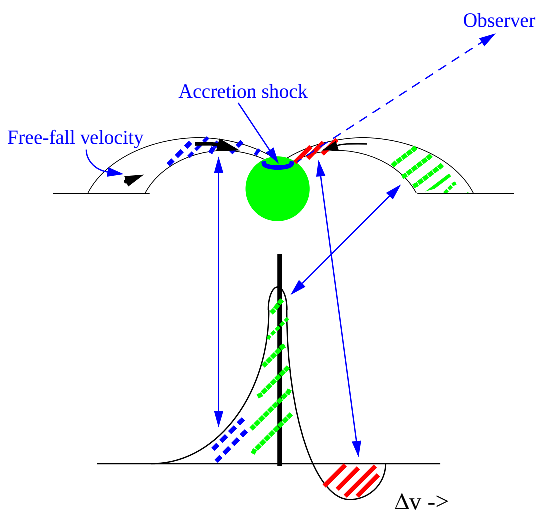

Fig. 3. Schematic of line formation in the magnetospheric accretion flow. Most flux at line center comes from the regions where matter is lifted from the disk, at nearly zero velocity. Blue-shifted emission comes from flow at the back of the star, falling in. Red-shifted emission is formed if the line of sight crosses the infalling material in front of the hot accretion shock.

of a magnetospheric model [38].

Broad line profiles characteristic of magnetospheric accretion have been identified in stars below the substellar limit, the brown dwarfs [39]. Because their low accretion luminosity yields little continuum flux excess, line profiles have been crucial in finding the accreting stars in the 10 Myr association TW Hya, other than in TW Hya itself [40, 41]. Finally, magnetospheric accretion as indicated by broad and nearly symmetric line profiles has been identified in protostars. Fig. 5 shows the observed Brγ profile of a protostar, PV Cep, together with the excellent fit with a magnetospheric model [42].

Empirical correlations between line luminosities and accretion luminosities for a sample of CTTS with well determined $\dot{M}$ from veiling studies have been found [43, 44]. These correlations can be used to determine the mass accretion rates in objects which are too extincted to be observed in the optical or in the UV. Using this method, accretion luminosities have been

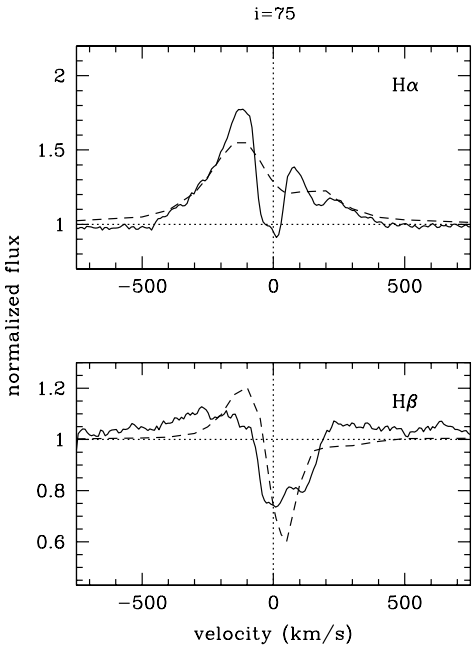

Fig. 4. Line profiles of Hα and Hβ of the Herbig Ae/Be star UX Ori (solid lines), compared to predictions of magnetospheric accretion models (dotted lines) ([38])

estimated for Class I objects [43]; it was found that L_{acc} is lower than the observed luminosity by at least by a factor of 10. Two consequences follow: (1) the observed luminosity in Class I must be due to stellar luminosity, and thus is not an accretion indicator, and (2) the typical mass accretion rate in the disks of protostars, $\sim 10^{-7} M_{\odot} yr^{-1}$, estimated from L_{acc}, is lower than the mass infall rate by roughly a factor of 10 (in Taurus). These facts have profound implications for the evolution of YSO (see Hartmann lectures).

5.2 The Accretion shock

Material falling along magnetic field lines will reach the stellar surface at free-fall velocities. It has to slow down through a shock to merge with the photosphere below. For typical parameters, the shock forms just above the stellar surface [45]. The total luminosity emitted by the accretion columns is $L_{shock} = \zeta L_{acc}$, where $\zeta = 1 - R_*/R_t$. So, for typical values of R_t/R_*, most of the accretion luminosity is emitted in the shock [45].

Soft X-rays from the shock heat the photosphere below it and the pre-shock region just above it along the accretion column. Roughly, 1/2 of

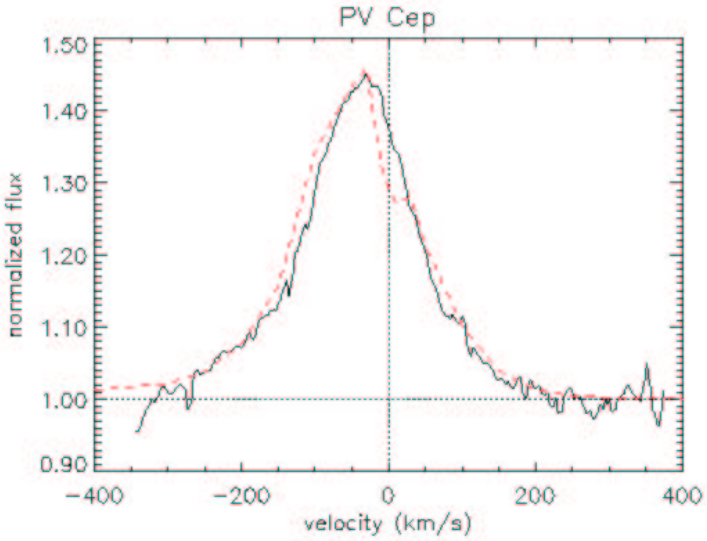

Fig. 5. Line profiles of Brγ in the Class I object PV Cep (solid line), compared to predictions of magnetospheric accretion models (dotted line) ([42])

L_{shock} is emitted in each direction. In turn, half of the energy entering the pre-shock is re-emitted down towards the heated photosphere, while the rest leaves the shock region. As a first approximation, the heated photosphere emits as a black body, with $\sigma T_{hp} \sim 3/4 L_{shock}/A \sim 3/4\mathcal{F}$, where $\mathcal{F}$ is the energy flux carried by each column and A is total surface area covered by accretion columns. The pre-shock region, on the other hand is optically thin with a temperature $\sim 10000 - 20000$K.

Accretion shock models based in these simple principles can explain very well the observed optical and UV excesses of CTTS [45, 46]. Typical energy fluxes carried by the accretion columns are found to be $\sim 1 - 3 \times 10^{11} \mathrm{erg\,s^{-1}\,cm^{-2}}$, with corresponding temperatures of the heated photosphere of the order of 7000 - 9000 K. The surface filling factor of the shock is found to be very small, < 1 %. The so-called continuum stars, those so heavily veiled that absorption lines are difficult to detect, carry similar energy fluxes in their accretion columns, but the filling factors are much higher, ~ 10 % [45, 46]. Line fluxes formed in the pre-shock region have been calculated for typical parameters, and found to compare well with

observations [47].

Shock emission has also been calculated for HAeBe. However, the *effects* of shock emission are much more difficult to discern in this case. The reason is that if the energy carried by accretion columns in HAeBe is similar to that of the lower mass CTTS, then the emission from the heated photosphere, which really stands out from the cool photospheres of CTTS, is now similar to that of the stellar photosphere. Standard de-veiling procedures applicable to CTTS cannot be implemented in HAeBe because of the differential veiling introduced by line formation in the heated photosphere [38]. One conspicuous indicator of accretion seems to be the Balmer jump, which tends to go from absorption to emission as the mass accretion rate increases. Comparison with observed strengths of Balmer jumps indicate mass accretion rates of the order of $10^{-8} - 10^{-7} M_{\odot} yr^{-1}$ for the disks of HAeBe [38].

In conclusion, the observed continuum excess in the optical and the UV in YSO can be explained fairly well with emission from the accretion shock. This justifies the measurement of the accretion luminosity from this excess, and thus the estimates of $\dot{M}$ on which the magnetospheric model is based.

6 Observations of disks in YSO

While the optical and UV flux excesses in CTTS arise in the region of interaction between the disk and the star, the disk itself is responsible for the flux excess at long wavelengths. The lack of correlation between the extinction A_V and the IR excess was interpreted long ago as due to a flat geometry [48], but it was not until the 1990's that disks were imaged directly with HST. Disk images seen dark against the nebular background in the so-called proplyds in the Orion Nebula Cluster [49] or in light scattered in the surface of edge-on disk [50] indicate the disks are flared rather than flat, with typical sizes 100 - 500 AU.

Disks around CTTS have also been imaged in the mm wavelength range, both in dust continuum emission [51, 52] and in molecular lines [53–55]. Velocity gradients measured in molecular observations are consistent with Keplerian velocity, which would be expected if disks were geometrically thin and moved in the central potential of the star. Disk masses have been estimated from the dust continuum emission, assuming that the disk is optically thin and that the disk is isothermal vertically. With these assumptions, the disk flux can be written as the sum of the emission of all annuli,

$$F_\nu = \frac{2\pi}{d^2} \int_{R_1}^{R_2} B_\nu(T(R)) \Sigma(R) \kappa_\nu R \, \mathrm{d}R \qquad (6.1)$$

where it has been used that the specific intensity at each annulus is $I_\nu = B_\nu(1 - exp(-\tau_\nu / \cos i) \sim B_\nu \tau_\nu / \cos i$, with B_ν the Planck function. The

optical depth is given by $\tau_\nu = \kappa_\nu \Sigma$, where κ_ν is the dust opacity. Assuming that the dependence of temperature and surface density on radius is given by power laws, $T = T_0(R/R_0)^{-q}$ and $\Sigma = \Sigma(R/R_0)^{-p}$, the observed flux is related to the disk mass $M_d = \int_{R_1}^{R_2} 2\pi\Sigma R\,\mathrm{d}R$ as

$$\nu F_\nu = \frac{4k\nu^3}{c^2}\kappa_{nu} M_d T(R_d) \left(\frac{2-p}{2-p-q}\right) \tag{6.2}$$

where $T(R_d)$ the temperature at the disk radius [5, 51]. With estimates for p, q, and the dust opacity, the measured flux gives the mass of the disk. Assuming $\kappa_\nu = \kappa_0(\nu/\nu_0)^\beta = \kappa_0(\lambda_0/\lambda)^\beta$,

$$\nu F_\nu \propto \nu^{3+\beta} \tag{6.3}$$

that is, the slope of the SED in the mm gives the frequency dependence of the opacity, under this approximations. The dust opacity frequently used gives $\kappa_0 = 0.1\mathrm{cm}^2\mathrm{gr}^{-1}$ at $\lambda_0 = 250\mu$m [58]. With this value, $M_d \sim 0.01 - 0.1\mathrm{M}_\odot$ [51], which indicates that indeed disk is less massive than the star.

In summary, to estimate the disk mass, we require knowledge of the dependences of T and Σ with radius, in addition to the dust opacity. Simplifying assumptions as those described are useful to get order of magnitude estimates, but more detailed treatments are needed to get more accurate estimates and to determine how accretion properties can be obtained from observations. Appropriate solutions of the disk structure equations are required to calculate the physical quantities. In addition, the dust opacity depends on the compounds, the grain size distribution, and the degree of dust settling in the disk. Results from more detailed treatments will be discussed below.

7 Accretion disks

Since disks in YSO are accreting, we attempt to describe them using the theories of accretion disks. Many excellent reviews and books on accretion disks have been published (cf. [29]) even specifically to the case of YSO [5]. I refer the reader to those for more details. In here, I will only list the basic properties of steady accretion disks.

Assume a disk with a differential rotational velocity, moving in the potential of a central star. If the disk is geometrically thin, the rotational velocity will be the Keplerian velocity, $\Omega_K = \sqrt{GM_*/R_*^3}$. Friction between nearby radii will release heat. As a result, the material loses energy and sinks in the potential well, drifting towards the star. At the same time, some material must move outwards to conserve angular momentum. So, matter drifts inwards and angular momentum outwards.

A geometrically thin accretion disk with a steady mass accretion rate $\dot{M}$ has a surface density distribution given by

$$\Sigma = \frac{\dot{M}}{4\pi\nu}\left[1 - \left(\frac{R_*}{R}\right)^{1/2}\right] \tag{7.1}$$

where ν is the viscosity, and a temperature distribution given by

$$T_{vis} = \left(\frac{3GM_*\dot{M}}{8\pi\sigma R^3}\left[1 - \left(\frac{R_*}{R}\right)^{1/2}\right]\right)^{1/4} \tag{7.2}$$

so, $T_{vis} \propto R^{-3/4}, R >> R_*$. If the disk is optically thick, the SED resulting from this temperature distribution is given by

$$\lambda F_\lambda \propto \lambda^{-4/3} \tag{7.3}$$

8 FU Ori objects

The FU Ori objects constitute a perfect example of the steady accretion disk. The first objects of these class were discovered by an increase in flux by 2-3 orders of magnitude over time scales of months, reaching luminosities of $100-1000 L_\odot$. In only one case a pre-outburst optical spectrum exists, and it was similar to that of a CTTS After the outburst, the spectrum changed to that of a $\sim$ G-F star. FU Ori objects are found in close association with molecular clouds in star-forming regions.

It is now accepted that FU Ori objects are high mass accretion rate disks surrounding a low mass YSO (see review [56, 57] and references therein). This interpretation naturally explains the observed features of the objects. Spectra at different wavelength ranges indicate that the spectral type becomes later with increasing wavelength. So, while the optical spectrum is similar to that of an F star, the spectrum at 2μm appears similar to that of a K supergiant. This property can be explained naturally by a disk, in which a range of temperatures is present (cf. eq.(7.2)). An accretion disk can also naturally explain the double-line profile of the lines, expected from a ring-like geometry, and moreover, it can explain the decrease of rotational velocity between the optical and the infrared, consistent with Keplerian velocity. Finally, the SED of the least embedded of these objects, FU Ori itself, is consistent with the expected emission from steady disks, eq.(7.3). In others, the disk emission is more contaminated by envelope emission and it is difficult to extract.

The properties of the disk can be inferred from the luminosity, obtained by integration of the observed fluxes, the measured rotational velocities, and the maximum temperature observed. These three conditions can be used

to infer the mass accretion rate, and the stellar properties (with certain uncertainty for the inclination). The mass accretion rates inferred are of the order of $10^{-5} - 10^{-4}\, M_{\odot} yr^{-1}$, much higher than the mean $\dot{M}$ of CTTS, and consistent with accretion luminosity dominating the emission over stellar luminosities.

Disk atmospheres with effective temperature equal to eq. (7.2) with these mass accretion rates and gravities corresponding to a geometrically thin disk in a central potential, can explain well the observed features of the spectrum. In particular, deep and broad near infrared CO bands at 2.2μm are a characteristic feature. As mentioned, the SED of all known FU Ori objects shows a contribution from surrounding envelope material. It is smaller in the first discovered visible objects, but other, heavily embedded FU Ori objects have only been discovered by the presence of deep CO absorption.

In the case of FU Ori objects, then, the total luminosity measures the accretion. However, independent confirmation of the existence of a disk with high mass accretion rate is required to assign an object to this class.

9 Irradiated accretion disks

In contrast to FU Ori objects, the SEDs of CTTS are much flatter than expected from eq. (7.3) [2, 59], which first raised questions about their accretion disk nature. We have seen that disks in CTTS are accreting mass at a rate given by $\dot{M} \sim 10^{-8} M_{\odot} yr^{-1}$, which results in an accretion luminosity of $< 0.1 L_{\odot}$, mostly released at the accretion shock on the surface. With $L_* \sim 1 L_{\odot}$, $L_* >> L_{acc}$, which means that stellar irradiation must play an important role in the heating of the disk [59]. In fact, they are irradiated accretion disks.

For a flat disk, the irradiation flux can be estimated as

$$F_{irr} \sim I_* \Omega_* \cos\theta \sim \frac{I_* \pi R_*^2}{R^2} \frac{h}{R} \propto I_* \left(\frac{R_*}{R}\right)^3 \tag{9.1}$$

where θ is the angle between the line from a representative point on the stellar surface to the point R in the disk and the line along the midplane, approximating the stellar radiation as coming in a single beam, and $h \sim R_*$ is the height of the representative point above the midplane. With $F_{irr} \sim \sigma T^4$, $T \propto R^{-3/4}$, similar to an accretion disk, and thus resulting in SEDs that cannot explain the observations either.

However, disks of CTTS are not flat, they are flared, which means that they can capture more stellar radiation than flat disks. In the case of a vertically isothermal, geometrically thin disk affected by the central potential of the star, the density can be found from the equation of hydrostatic equilibrium in the vertical direction to be

$$\rho(z, R) = \rho_c e^{-\frac{z^2}{2H^2}} \tag{9.2}$$

where $\rho_c(R)$ is the density at the midplane and H is the scale height, given by

$$H = \frac{c_s}{(GM_*/R^3)^{1/2}} = \frac{c_s}{\Omega_K} \propto T^{1/2} \tag{9.3}$$

where $c_s = (2kT/m)^1/2$ is the sound speed and m the mass of the particle. If T increases, the cross section to capture of stellar photons increases, so the disk gets heated. A stable solution for the disk surface exists, corresponding to a flared surface [59, 60]. In these solutions, $T(R) \rightarrow R^{-1/2}$, and the corresponding SEDs are much flatter than those of the purely viscous disk.

Disks are not vertically isothermal. Stellar radiation enters the disk at an angle θ_0 to the local normal, (again approximating the stellar radiation as coming in a single beam), so the energy captured by the disk is $\sim (\sigma T_*^4/\pi)(R_*/R)^2\mu_0$, with $\mu_0 = \cos\theta_0$ [61–65]. As stellar flux enters the disk, a fraction $d\tau_*/\mu_0$ is absorbed at each z, where τ_* is the optical depth at the wavelength range characterizing the stellar energy (the "stellar" range). This energy re-emerges at the wavelength characterizing the local temperature (the "disk" range). So, the stellar flux decreases with height. The main opacity source in CTTS disks is due to dust grains, because temperatures are low enough that dust is not sublimated. Dust opacity increases as λ decreases, and stellar radiation is emitted at a shorter wavelength than the radiation emitted by the disk, so the hotter the star, the larger the opacity at the stellar range and thus the heating.

The vertical temperature profile can be obtained from the equation of conservation of energy

$$\int \kappa_\nu B_\nu(T)\,\mathrm{d}\nu - \int \kappa_\nu J_d\,\mathrm{d}\nu = \frac{\mathrm{d}}{\mathrm{d}z}F_d \tag{9.4}$$

where κ_ν is the monochromatic opacity, J_d the mean intensity of the local radiation at the disk wavelength range, and F_d the local flux. Neglecting viscous heating, the local flux only changes by deposition of stellar energy, so

$$\frac{\mathrm{d}}{\mathrm{d}z}F_d \sim 4\pi\kappa^*\rho J_* = 4\pi\kappa^*\rho J_{*,0}e^{-\tau_*/\mu_0} \tag{9.5}$$

where κ^* is the opacity at the stellar wavelength, and $J_{*,0}$ is the mean intensity entering the disk. With $J_{*,0} = 1/4\pi \int I\,\mathrm{d}\Omega \sim I_*\Omega_*/4\pi$,

$$\kappa_P(T)\frac{\sigma T^4(z)}{\pi} = \kappa_P(T)J_d(z) + \kappa_P(T_*)\frac{\sigma T_*^4}{\pi}\left(\frac{R_*}{R}\right)^2 e^{-\tau_*/\mu_0} \tag{9.6}$$

with $\kappa^* \sim \kappa_P(T_*)$, and κ_P the Planck mean opacity ([65, 66]).

In the surface, where the local field is much smaller than the stellar field, $J_d << J_{*,0}$, and $\tau_*/\mu_0 << 1$,

$$\kappa_P(T_0)T_0^4(z) \sim \kappa_P(T_*)T_*^4\left(\frac{R_*}{R}\right)^2 \tag{9.7}$$

This is the expression for the surface temperature T_0, given by the optically thin limit. Note that this is the "hot layer" temperature in the 2-level approximation [64].

Stellar heating and thus the temperature decrease as radiation penetrates the disk, because the optical depth increases (cf. eq.(9.6)). The actual T profile depends on μ_0, that is, on the actual shape of the *surface* of the disk, defined as the surface where $\tau_*/\mu_0 \sim 1$, that is, where most of the stellar energy is deposited. The size of the upper optically thin region above the surface is given by $\Delta z \sim \mu_0/\kappa^*$; the more inclined the surface, the smaller the optically thin region.

Results of the detailed solution of the set of equations of vertical structure including viscous dissipation for a disk with typical CTTS parameters are shown in Fig. 6 [66]. The Figure on the right shows the height of the surface, z_s, the scale height H, and the photospheric height z_{phot}, where the Rosseland mean optical depth $\tau_{Ross} \sim 1$. Since the opacity at the wavelength where the stellar radiation is absorbed ($\lambda_* \sim 1\mu$m for $T_* \sim 4000$K), is large, the surface is flared out to a few hundred AU, even though the disk becomes optically thin to its own radiation ($\tau_{Ross} < 1$) at ~ 20 AU.

The left side of Fig. 6 shows characteristic temperatures in the disk. It can be seen that the midplane temperature T_m is higher than the photospheric temperature $T_{phot} = T(z_{phot})$ in the inner disk, where it is optically thick to its own radiation. This can be understood using the diffusion approximation

$$\frac{\mathrm{d}}{\mathrm{d}z} J_d = \frac{\mathrm{d}}{\mathrm{d}z} \sigma T^4 = -\frac{3}{4\pi} \chi_R \rho F_d \tag{9.8}$$

from which we can write approximately

$$\Delta(\sigma T^4) \sim \frac{3}{4\pi} \tau_R F_d \tag{9.9}$$

In the inner annuli, $\tau_R >> 1$, $T_m > T_{phot}$; the temperature gradient allows the flux (viscous plus local radiation) to emerge from the disk. In contrast, when the disk becomes optically thin to its own radiation, $\tau_R << 1$, the disk becomes nearly isothermal in the regions near the midplane. On the other hand, the surface temperature T_0 is higher than T_{phot} in the inner regions and than T_m when the disk becomes optically thin in the outer regions, as predicted by eq.(9.6). By comparison of T_m and T_{vis} in Fig. 6, it can be seen that viscous heating is only important near the midplane of the regions inside 1 AU, given the low $\dot{M}$ characteristic of the the typical CTTS. Finally, it can be seen that temperatures behave as $1/R^{1/2}$ for $R >> R_*$.

This particular shape of the temperature profile has important observational implications. For one thing, features formed in the optically thin upper regions will appear in emission, even if the disk is optically thick, because the local temperature is so much higher than that of deeper regions

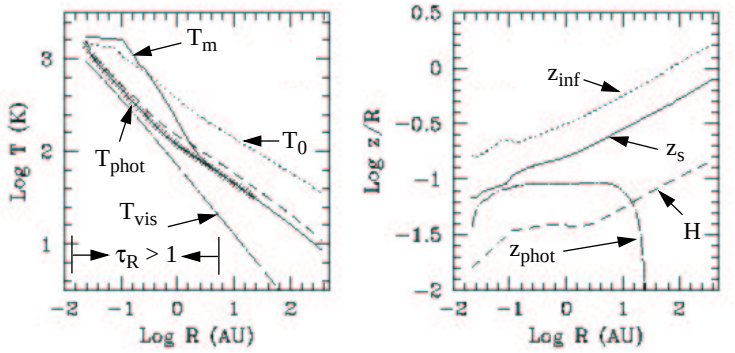

Fig. 6. Left: Characteristic temperatures in the disk: midplane temperature (T_m), surface temperature (T_0), photospheric temperature (T_{phot}), and viscous temperature (T_{vis}). The disk is optically thick (to its own radiation, $\tau_R > 1$) inside ~ 6 AU. Right: Characteristic heights in the disk: surface (z_s), scale height (H), photospheric height z_{phot} (defined in regions where the disk is thick to its own radiation). z_{inf} is the top height of the disk. The disk model parameters are $M_* = 0.5\mathrm{M}_\odot$, $R_* = 2\mathrm{R}_\odot$, $T_* = 4000K$ and $\dot{M} = 10^{-8} M_\odot yr^{-1}$. Adapted from [66].

where the continuum forms. These includes strong features like the CO near infrared lines or the silicate features [61, 62, 67]. The higher temperatures of the upper layers also imply that molecules can exist in the gas phase in the disk, even when the midplane temperatures are so low that molecules are settled onto grains surfaces [69–71]. For example, if the disk shown in Fig. 6 was isothermal at T_m, the CO molecules would be on grains surfaces for $R > 60AU$, for which $T < 20$K. However, the hot upper layers are kept at a temperature high enough for molecules to be in the gas phase out to ~ 400AU, in agreement with mm molecular observations [53–55].

The surface density of the disk can be self-consistently calculated from the disk equations. The limiting behavior can be obtained from eq.(7.1). In the parametric α prescription [72], the viscosity can be written as $\nu = \alpha c_s H = \alpha c_s^2/\Omega_K$, using eq.(9.3). With $c_s \propto T^{1/2} \propto R^{-1/4}$ and $\Omega_K \propto$

$R^{-3/2}$, we obtain at large radii

$$\Sigma \sim 4 \left(\frac{\dot{M}}{10^{-8}\frac{\mathrm{M}_\odot}{\mathrm{yr}}}\right)\left(\frac{\alpha}{0.01}\right)^{-1}\left(\frac{T_{100\,AU}}{10K}\right)^{-1}\left(\frac{R}{100AU}\right)^{-1} \mathrm{gr\ cm}^{-2} \quad (9.10)$$

using values of α found in modeling CTTS disks and expected from theories [73], and typical temperatures at 100 AU. The surface density dependence on radius of irradiated accretion disks, $\propto 1/R$, is much flatter then the usually assumed dependence $p = 3/4$, and it has been confirmed by observations [74].

Supposing this dependence holds at all radii, the disk mass is given by

$$M_d = 0.03\ \frac{\left(\frac{\dot{M}}{10^{-8}\frac{\mathrm{M}_\odot}{\mathrm{yr}}}\right)\left(\frac{R_d}{200\,AU}\right)^{1/2}}{\left(\frac{\alpha}{0.01}\right)\left(\frac{M_*}{0.5\mathrm{M}_\odot}\right)^{1/2}\left(\frac{T_{Rd}}{10K}\right)}\ \mathrm{M}_\odot \quad (9.11)$$

in agreement with values determined from dust mm emission. Therefore, the mass accretion rates determined from the inner disk properties are consistent with large-scale properties like the disk mass. Note that if $\dot{M}$ is known for a given star, then M_d and α are complementary parameters, since the temperature at the outer disk radii, T_{Rd} is fixed by stellar irradiation and sizes can be estimated from observations.

10 Effects of dust properties

The expression normally used to calculate the disk flux is eq. (6.1), with $I_\nu = B_\nu[1-exp(-\tau_\nu/\cos i)]$ to account for optically thick emission. However, this expression is a simplification of the actual situation. As we have seen, the temperature and surface density profiles in the disk are not power laws, and disks are not vertically isothermal. In addition, since actual disks are flared, emission from the innermost disk annuli may be attenuated by the outer disk for certain ranges of inclination [66].

Nonetheless, eq. (6.1) shows the main effects. In particular, it indicates that the SED is highly dependent on the properties of the dust, because it depends explicitly on κ_ν and on the temperature structure, which as we have seen is determined by the dust opacity. It is then important to understand the effects of dust.

The dust opacity depends on the shape, size distribution, and constitution of the dust grains. Schematically, a spherical grain of size a will have a cross section to radiation of wavelength λ of the order of the geometrical cross section πa^2, if $\lambda << 2\pi a$, but the cross section will decrease as $\sim \lambda^{-2}$ for $\lambda >> 2\pi a$. The dust opacity, in $\mathrm{cm}^2\mathrm{gr}^{-1}$, will be given by the cross section over the mass of the grain, $\rho_g 4/3\pi a^3$, where ρ_g is the density of

the grain, so it will be proportional to $1/a$. So, the bigger the grain, the lower the opacity at short wavelengths and the higher at long wavelengths, $\lambda \leq 2\pi a$, because the transition to the λ^{-2} regime occurs at longer wavelengths. This is shown as shown schematically in Fig. 7 for grains of sizes a_1 and a_2, $a_1 < a_2$.

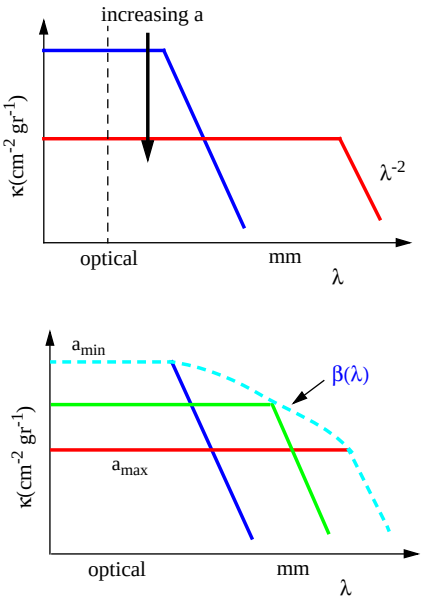

Fig. 7. Dependence of opacity on grain size. Upper: opacity for single grains. As the grain size a increases, κ decreases at short λ, and increases at long λ. Lower: opacity for a grain size distribution. The slope β of κ vs. λ depends on λ.

A simple characterization of the dust can be done by assuming that the dust particles are homogeneous spheres with a size distribution, $n(a)da = a^{-p}da$, where a is the grain size and the exponent p is usually taken as 3.5, describing the properties of the interstellar medium dust [75], or 2.5, if there has been some degree of coagulation [76]. Additional parameters are the minimum and maximum sizes, a_{min} and a_{max}. If a_{min} and the amount of dust are fixed, the larger the a_{max} the less the smaller particles, because the larger particles take more mass. Therefore, the lower the opacity at short

wavelengths and the higher at long wavelengths. For a mixture of sizes, the transition from the "flat" to the $\propto \lambda^{-2}$ regime occurs over a large range of wavelengths (see Fig. 7), so that the local slope of the function $\kappa(\lambda)$ changes slowly from ~ 0 to ~ -2. Therefore, the form usually assumed to represent the dust opacity $\kappa \propto \lambda^{-\beta}$ is not actually valid, since β depends on λ [68,76], although it may be applicable over for a sufficiently small λ interval.

The surface of the disk, that is, the height where the stellar radiation is absorbed, depends on the dust opacity. For instance, a dust mixture characterized by $a_{max} \leq 1\mu$m will result in more absorption of stellar radiation, at $\lambda \sim 1\mu$m, that one characterized by $a_{max} \sim 1$ mm. Therefore, the resultant surface will be higher for the lower a_{max} case. Since the flux absorbed by the disk depends on the inclination of the surface through μ_o, more stellar radiation is absorbed as the disk gets more flared and the hotter the disk will get, resulting in higher infrared fluxes for smaller a_{max}. On the other hand, the mm emission of the $a_{max} \leq 1\mu$m disk will be lower than that of the $a_{max} \sim 1$ mm disk, because larger grains are more efficient emitters at those wavelengths. Therefore, the SED gives direct information of the dust properties. In particular, the median SED of the CTTS in Taurus can be much better explained by $a_{max} \sim 1$ mm dust than by interstellar medium dust [68].

11 SEDs of HAeBe

The $\dot{M}$ inferred from magnetospheric and shock analysis of (visible) HAeBe are similar to those in CTTS. However, the disks are expected to be hotter since the effective temperatures and luminosities of the central stars are higher. SEDs of HAeBe surrounded by disks including these effects can explain well the observations [67]. However, they cannot explain the "bump" at 2-3μm, which has been a puzzle for almost 10 years.

Early interpretations of the SEDs of HAeBe required high mass accretion rates $\dot{M} \sim 10^6 M_\odot yr^{-1}$ to explain the "bump", that is, the high fluxes at 2-3μm. On the other hand, they also required holes in the disk of the order of 0.1-1 AU to explain the lack of emission at shorter wavelengths [4]. The hole was generally located at the radius where the dust would be destroyed, R_{dust}. However, it was soon recognized that with such high $\dot{M}$ the inner gas disk would be optically thick and thus still have large emission at J [77].

A breakthrough came with the realization that if the dust disk had some vertical size, then the disk would show a wall facing the star at the dust destruction radius. In this wall, radiation from the star would enter frontally, and thus it would be much hotter than the surface of the disk. Radiation from this wall can explain very well the extra emission [67, 78]. Even with the lower $\dot{M}$ we now expect for the HAeBe, the inner gaseous disk will be marginally thick, but the scale height in those regions is low

enough for radiation to reach the dust wall [38].

12 Winds as accretion diagnostics

YSO are losing matter. Powerful outflows in molecular and atomic material are observed in objects still surrounded by infalling envelopes. In the visible CTTS, they show through blue-shifted absorption components in the permitted emission lines and in forbidden line emission.

Many models have been presented for the origin of the winds in YSO, as discussed by other lectures in these classes. They all have in common the hypothesis that winds are powered by accretion. This hypothesis is confirmed by observations. In particular, the equivalent width of the forbidden line [OI], expected to form in the low density regions of the wind, correlates well with accretion indicators as veiling and with K-L excesses [5, 7]. Moreover, the luminosity of [OI] correlates very well with the accretion luminosity [81]. In addition, the strength of the blueshifted absorption components in the emission lines increases with $\dot{M}$, such that the emission disappears in the objects with the highest $\dot{M}$, the FU Ori objects. In these objects, the mass accretion is so high that the magnetosphere, where the emission is formed, is quenched (cf. eq.(5.1)).

Models differ in the location where the wind forms. In broad terms, the wind either arises in the so-called X-region, located at the corotation radius [32] or it originates in a wider region in the disk [80]. It is difficult to find observational diagnostics that help discriminate between models. I will not discuss them here; rather, I will refer to a case in which the origin of the wind can be proven to be in the disk, the FU Ori objects.

As I mentioned, absorption lines formed in a disk have well defined double-peaked profiles. These profiles have been observed in mm molecular lines in CTTS, which are formed in the outermost regions, where dust opacity is very low. However, the hot inner gaseous annuli of FU Ori objects produce spectrum rich in metallic absorption lines, in which the characteristic disk profile shows very well. Nonetheless, not all lines are double in FU Ori. The strongest lines, generally located in the blue region of the spectrum, are single and blueshifted [82]. This is a direct consequence of the presence of a disk wind. If material is leaving the disk surface, it is expected to accelerate until it gets to a terminal velocity at several scale heights above the midplane. Weak lines will form on the disk surface and will be broadened by the rotational velocity of the disk, so they will be double. Strong lines will form much higher, where the expansion velocity dominates over rotation, so they will be single and blueshifted [83]. Therefore, the observed behavior of the lines gives clear indication of the presence of a disk wind. Modeling of the lines has yield the mass loss rate of this wind [83].

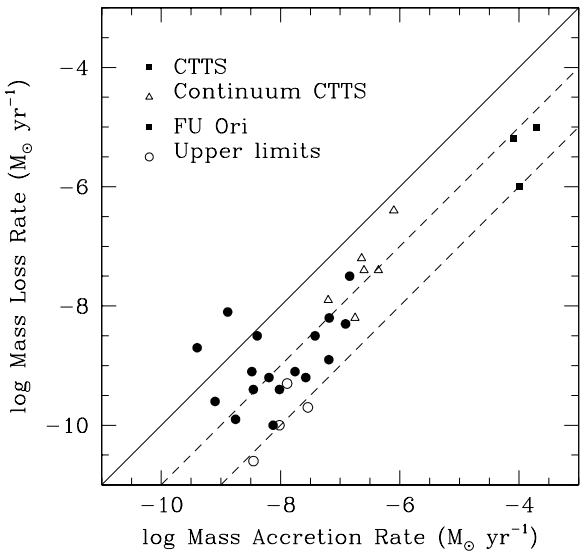

Fig. 8. Mass loss rate vs. mass accretion rate for YSOs. Different type of objects are indicated in the Figure.

In CTTS, mass loss rates have been estimated from the measured fluxes and velocities of the forbidden lines, with various assumptions for the temperature and geometry [7]. Fig. 8 shows the mass loss rate vs. the mass accretion rate for several types of YSO. It includes the CTTS, the more active, heavily veiled "continuum" CTTS, and the FU Ori objects. A remarkable correlation shows holding over 4-5 orders of magnitude of the mass accretion and loss rates, and it suggests a similar origin for the winds in all objects. In any event, this correlation indicates that the presence and strength of a wind is an important accretion diagnostic. Objects with strong winds must be powered by accretion disks where matter is accreted at a rate ~ 10 higher than the mass at which matter is being lost.

13 Validity of the models

We have seen that a model based on accretion of matter onto the star can explain the observed properties of YSO. The model includes an irradiated accretion disk, from which $\sim 10\%$ of the matter is lost in the wind, and

the rest falls onto the star along magnetic field lines, merging with the photosphere through an accretion shock.

The models are axially symmetric, uniform, and assume the simplest geometry for the magnetic field. Reality is much more complicated than this.

First of all, a large degree of variability is observed in both lines and continua. This variability is nearly periodic in visual and red optical bands, as is interpreted as rotational modulation of spots in the surface ([85–87], in a configuration where the magnetic field axis is inclined relative to the rotation axis.

In addition, the magnetospheric flow probably is not axially symmetric. The observed correlation between line luminosities and accretion luminosities cannot be explained by axially symmetric models, which predict higher fluxes than observed at the lowest values of $\dot{M}$. However, it can be understood if the area covered by accreting columns decreases with $\dot{M}$, as suggested by the comparison of shock emission between normal CTTS and the continuum stars [37]. To support this, accretion by sectors is required to explain the line profile of very low mass objects with extremely low values of $\dot{M}$ [39].

The magnetospheric sectors are probably not uniform in density or temperature either. Broad velocity wings are observed in lines requiring high temperatures as the C IV lines [88], indicating that they form in the extended flow. So, it appears that high and low temperature coexist in the flow.

Similarly, disks may not be axisymmetric. Absorption episodes, as observed in the UX Ori objects [67], and in some CTTS [89] may be due to warps in the disk [90]. Nor is dust homogeneously distributed in the disk, radially or vertically.

Given all these facts, it is remarkable that models so simple can explain such a large range of observations, from the ultraviolet to the mm range. This may indicate the models contain the essential physics of the problem, namely, accretion as the main mechanism driving the activity.

14 Summary

To briefly summarize these lectures, accretion is taking place in YSO. In protostars, it occurs in two stages, from cloud to disk, and from disk to star. The observed luminosity of protostars is not due to energy released in the infall from the cloud, because matter lands on the disk too far from the star. In general, it is due to the stellar luminosity. There are cases of high $\dot{M}$ disks in which $L_{obs} \sim L_{acc}$, but independent confirmation of the existence of such disks, as deep near IR CO absorption bands, is required to confirm the assumption. In the accreting TTS, the CTTS, magnetospheric accretion

transfers mass from the disk onto the star. This is indicated by broad emission lines formed in the accretion flow, and by excess continuum emission in the optical and UV, due to accretion shock emission. Measurements of this excess yield L_{acc}. Correlations of luminosities in the U band and of optical and IR lines with L_{acc} are useful to obtain L_{acc} for large samples and/or heavily extincted stars. Although CTTS are surrounded by accretion disks, the emission properties of these disks do not provide a direct measurement of the mass accretion rate, because for the average $\dot{M} \sim 10^{-8} M_{\odot} yr^{-1}$ of CTTS , stellar irradiation dominates the heating.

I would like to thank the organizers for the invitation to participate in the Summer School and the European Union for sponsoring the visit. I also would like to thank Bruno Merin for valuable comments to the manuscript. Work reported in these lectures was supported by NASA grant NAG5-4282.

References

[1] Siess, L., Dufour, E., & Forestini, M., "An internet server for pre-main sequence tracks of low- and intermediate-mass stars", AA 358 (2000) 593-599.

[2] Kenyon, S. J. and Hartmann, L., "Pre-Main-Sequence Evolution in the Taurus-Auriga Molecular Cloud", ApJS 101 (1995) 117-171.

[3] Briceño, C., Luhman, K.

[4] Hillenbrand, L. A.; Strom, St. E.; Vrba, F. J.; Keene, J., "Herbig Ae/Be stars - Intermediate-mass stars surrounded by massive circumstellar accretion disks", ApJ 397 (1992) 613-643.

[5] Hartmann, L., "Accretion processes in star formation", (1998), New York : Cambridge University Press.

[6] Herbig, G. H.; Bell, K. Robbin, "Catalog of emission line stars of the orion population", (1988), Lick Observatory Bulletin, Santa Cruz.

[7] Hartigan, P.; Edwards, S.; Ghandour, L., ApJ 452 (1995) 736-768.

[8] Costa, V. M.; Lago, M. T. V. T.; Norci, L.; Meurs, E. J. A, "T Tauri stars: The UV/X-ray connection", AA 354 (2000) 621-635.

[9] Neuhaeuser, R.; Sterzik, M. F.; Schmitt, J. H. M. M.; Wichmann, R. and Krautter, J., "ROSAT survey observation of T Tauri stars in Taurus", AA 297 (1995) 391-417.

[10] Folha, D. F. M.; Emerson, J. P., "High veiling at near infrared wavelengths in classical T Tauri stars", AA 352 (1999) 517-531.

[11] Lynden-Bell, D.; Pringle, J. E., "The evolution of viscous discs and the origin of the nebular variables", MNRAS 168 (1973) 603-637.

[12] Johns-Krull, C. M.; Valenti, J. A.; Koresko, C., "Measuring the Magnetic Field on the Classical T Tauri Star BP Tauri", ApJ 516 (1999), 900-915.

[13] Guenther, E. W.; Lehmann, H.; Emerson, J. P.; Staude, J., "Measurements of magnetic field strength on T Tauri stars", AA 341 (1999) 768-783

[14] Johns-Krull, C. M.; Valenti, J. A.; Hatzes, A. P.; Kanaan, A., "Spectropolarimetry of Magnetospheric Accretion on the Classical T Tauri Star BP Tauri", ApJ 510 (1999) L41-L44.

[15] Hartmann, L.; Hewett, R.; Stahler, S.; Mathieu, R. D., "Rotational and radial velocities of T Tauri stars", ApJ 309 (1986) 275-293.

[16] Bouvier, J.; Bertout, C.; Benz, W.; Mayor, M., "Rotation in T Tauri stars. I - Observations and immediate analysis", AA 165 (1986) 110-119.

[17] Zhou, S.; Evans, N. J., II; Wang, Y.; Peng, R.; Lo, K. Y., "A C(18)O survey of dense cores in the Taurus molecular cloud: Signatures of evolution and protostellar collapse", ApJ 433 (1994) 131-148.

[18] Mardones, D., "Signatures of Infall in Regions of Low Mass Star Formation", PhD Thesis, Harvard University (1998)

[19] Wilking, B. A. and Lada, C. J., "The discovery of new embedded sources in the centrally condensed core of the Rho Ophiuchi dark cloud - The formation of a bound cluster", ApJ 274 (1983), 698-716.

[20] Goodman, A. A.; Benson, P. J.; Fuller, G. A.; Myers, P. C., "Dense cores in dark clouds. VIII - Velocity gradients", ApJ 406 (1993) 528-547.

[21] Cassen, P.; Moosman, A., "On the formation of protostellar disks", Icarus 48 (1981) 353-376.

[22] Terebey, S.; Shu, F. H.; Cassen, P., "The collapse of the cores of slowly rotating isothermal clouds", ApJ 286 (1984) 529-551.

[23] Stahler, S. W., "Deuterium and the stellar birthline", ApJ 332 (1988) 804-825.

[24] Hartmann, L.; Cassen, P.; Kenyon, S. J., "Disk Accretion and the Stellar Birthline", ApJ 475 (1997) 770-785.

[25] Kenyon, S. J.; Calvet, N.; Hartmann, L., "The embedded young stars in the Taurus-Auriga molecular cloud. I - Models for spectral energy distributions", ApJ 414 (1993) 676-694.

[26] Kenyon, S. J.; Hartmann, L. W.; Strom, K. M.; Strom, S. E., "An IRAS survey of the Taurus-Auriga molecular cloud", AJ 99 (1990) 869-887.

[27] Gullbring, E.; Hartmann, L.; Briceño, C.; Calvet, N., "Disk Accretion Rates for T Tauri Stars", ApJ 492 (1998) 323-341.

[28] Hartmann, L.; Calvet, N.; Gullbring, E.; D'Alessio, P., "Accretion and the Evolution of T Tauri Disks", ApJ 495 (1998) 385-400.

[29] Frank, J.; King, A.; Raine, D., "Accretion power in astrophysics", UK: Cambridge University Press (2002)

[30] Ghosh, P.; Lamb, F. K., "Accretion by rotating magnetic neutron stars. III - Accretion torques and period changes in pulsating X-ray sources", ApJ 234 (1979) 296-316.

[31] Camenzind, M., "Magnetized Disk-Winds and the Origin of Bipolar Outflows", Reviews in Modern Astronomy 3 (1990) 234-265.

[32] Shu, F.; Najita, J.; Ostriker, E.; Wilkin, F.; Ruden, S.; Lizano, S., "Magnetocentrifugally driven flows from young stars and disks. 1: A generalized model", APJ 429 (1994) 781-796.

[33] Bertout, C.; Basri, G.; Bouvier, J., "Accretion disks around T Tauri stars", ApJ 330 (1988) 350-373.

[34] Muzerolle, J.; Hartmann, L.; Calvet, N., "Emission-Line Diagnostics of T Tauri Magnetospheric Accretion. I. Line Profile Observations", AJ 116 (1998) 455-468.

[35] Hartmann, L.; Avrett, E. H.; Loeser, R.; Calvet, N., "Winds from T Tauri stars. I - Spherically symmetric models", ApJ 349 (1990) 168-189.

[36] Calvet, N.; Hartmann, L.; Hewett, R., "Winds from T Tauri stars. II - Balmer line profiles for inner disk winds", ApJ 386 (1992) 229-238.

[37] Muzerolle, J.; Calvet, N.; Hartmann, L., "Emission-Line Diagnostics of T Tauri Magnetospheric Accretion. II. Improved Model Tests and Insights into Accretion Physics", ApJ 550 (2001) 944-961.

[38] Muzerolle, J., D'Alessio, P., Calvet, N.; Hartmann, L., in preparation.

[39] Muzerolle, J.; Briceño, C.; Calvet, N.; Hartmann, L.; Hillenbrand, L.; Gullbring, E., "Detection of Disk Accretion at the Substellar Limit", ApJ 545 (2000) L141-L144.

[40] Muzerolle, J.; Calvet, N.; Briceño, C.; Hartmann, L.; Hillenbrand, L., "Disk Accretion in the 10 MYR Old T Tauri Stars TW Hydrae and Hen 3-600A", ApJ 535 (2000) L47-L50.

[41] Muzerolle, J.; Hillenbrand, L.; Calvet, N.; Hartmann, L.; Briceño, C., "Disk Accretion at 10 Myr: Results from the TW Hydrae Association", Young Stars Near Earth: Progress and Prospects, ASP Conference Series Vol. 244. Edited by Ray Jayawardhana and T. Greene. San Francisco: Astronomical Society of the Pacific

[42] Muzerolle, J.; Calvet, N.; Hartmann, L., in preparation.

[43] Muzerolle, J.; Hartmann, L.; Calvet, N., "A Brgamma Probe of Disk Accretion in T Tauri Stars and Embedded Young Stellar Objects", AJ 116 (1998) 2965-2974.

[44] Calvet, N.; Hartmann, L.; Strom, S. E., "Evolution of Disk Accretion", Protostars and Planets IV, Tucson: University of Arizona Press; eds Mannings, V., Boss, A.P., Russell, S. S. (2000), 37.

[45] Calvet, N.; Gullbring, E., "The Structure and Emission of the Accretion Shock in T Tauri Stars", ApJ 509 (1998) 802-818.

[46] Gullbring, E.; Calvet, N.; Muzerolle, J.; Hartmann, L., " The Structure and Emission of the Accretion Shock in T Tauri Stars. II. The Ultraviolet-Continuum Emission", ApJ 544 (2000) 927-932.

[47] Gomez de Castro, A. I.; Lamzin, S. A, "Accretion shocks in T Tauri stars: diagnosis via semiforbidden ultraviolet line ratios", MNRAS 304 (1999) L41-L45.

[48] Cohen, M.; Kuhi, L. V., "Observational studies of pre-main-sequence evolution", ApJS 41 (1979) 743-843.

[49] O'dell, C. R., "Observational properties of the Orion Nebula proplyds", AJ 115 (1998) 263-273.

[50] Stapelfeldt, K. R.; Krist, J. E.; Menard, F.; Bouvier, J.; Padgett, D. L.; Burrows, C. J., "An Edge-On Circumstellar Disk in the Young Binary System HK Tauri", ApJ 502 (1998) L65-L69

[51] Beckwith, S. V. W.; Sargent, A. I.; Chini, R. S.; Guesten, R., "A survey for circumstellar disks around young stellar objects", AJ (99) 924-945.

[52] Dutrey, A.; Guilloteau, S.; Duvert, G.; Prato, L.; Simon, M.; Schuster, K.; Menard, F., "Dust and gas distribution around T Tauri stars in Taurus-Auriga. I. Interferometric 2.7mm continuum and 13CO J=1-0 observations", AA 309 (1996) 493-504.

[53] Dutrey, A.; Guilloteau, S.; Prato, L.; Simon, M.; Duvert, G.; Schuster, K.; Menard, F., "CO study of the GM Aurigae Keplerian disk", AA 338 (1998) L63-L66.

[54] Guilloteau, S.; Dutrey, A., "Physical parameters of the Keplerian protoplanetary disk of DM Tauri", AA 339 (1998) 467-476.

[55] Qi, C., "Aperture synthesis studies of the chemical composition of protoplanetary disks and comets", PhD Thesis, California Institute of Thechnology (2001).

[56] Hartmann, L.; Kenyon, S. J., "On the nature of FU Orionis objects", ApJ 299 (1985) 462-478.

[57] Hartmann, L.; Kenyon, S. J., "The FU Orionis Phenomenon", Annual Review of Astronomy and Astrophysics 34 (1996) 207-240.

[58] Beckwith, S. V. W.; Sargent, A. I., "Particle emissivity in circumstellar disks", ApJ (381) 250-258

[59] Kenyon, S. J.; Hartmann, L., "Spectral energy distributions of T Tauri stars - Disk flaring and limits on accretion", ApJ 323 (1987) 714-733.

[60] D'Alessio, P.; Cantó, J.; Hartmann, L.; Calvet, N.; Lizano, S., "On the Thermal Stability of Irradiation-dominated Pre-Main-Sequence Disks", ApJ 511 (1999) 896-903.

[61] Calvet, N.; Patiño, A.; Magris, G. C.; D'Alessio, P., "Irradiation of accretion disks around young objects. I - Near-infrared CO bands", ApJ 380 (1991) 617-630.

[62] Calvet, N.; Magris, G. C.; Patiño, A.; D'Alessio, P., "Irradiation of Accretion Disks around Young Objects. II. Continuum Energy Distribution", Rev. Mex. Astron. Astrofis. 24 (1992), 27-42.

[63] Malbet, F.; Bertout, C., "The vertical structure of T Tauri accretion disks. I - Heating by the central star", ApJ 383 (1991) 814-819.

[64] Chiang, E. I.; Goldreich, P., "Spectral Energy Distributions of T Tauri Stars with Passive Circumstellar Disks", ApJ 490 (1997) 368-376.

[65] D'Alessio, P.; Canto, J.; Calvet, N.; Lizano, S., "Acretion Disks around Young Objects. I. The Detailed Vertical Structure", ApJ 500 (1998) 411-427.

[66] D'Alessio, P.; Calvet, N.; Hartmann, L.; Lizano, S.; Cant, J., "Accretion Disks around Young Objects. II. Tests of Well-mixed Models with ISM Dust", ApJ 527 (1999) 893-909.

[67] Natta, A.; Prusti, T.; Neri, R.; Wooden, D.; Grinin, V. P.; Mannings, V., "A reconsideration of disk properties in Herbig Ae stars", AA 371 (2001) 186-197.

[68] D'Alessio, P.; Calvet, N.; Hartmann, L., "Accretion Disks around Young Objects. III. Grain Growth", ApJ 321 (2001) 321-334.

[69] Willacy, K.; Langer, W. D., "The Importance of Photoprocessing in Protoplanetary Disks", ApJ 544 (2000) 903-920.

[70] van Zadelhoff, G.-J.; van Dishoeck, E. F.; Thi, W.-F.; Blake, G. A., "Submillimeter lines from circumstellar disks around pre-main sequence stars", AA 377 (2001) 566-580.

[71] Aikawa, Y.; van Zadelhoff, G. J.; van Dishoeck, E. F.; Herbst, E., "Warm molecular layers in protoplanetary disks", AA 386 (2002) 622-632.

[72] Shakura, N. I. & Sunyaev, R. A., "Black holes in binary systems. Observational appearance", AA 24 (1973) 337-355.

[73] Stone, J. M.; Gammie, C. F.; Balbus, S. A.; Hawley, J. F., "Transport Processes in Protostellar Disks", Protostars and Planets IV, Tucson: University of Arizona Press; eds Mannings, V., Boss, A.P., Russell, S. (2000) 589

[74] Wilner, D. J.; Ho, P. T. P.; Kastner, J. H.; Rodrguez, L. F., "VLA Imaging of the Disk Surrounding the Nearby Young Star TW Hydrae", ApJ 534 (2000) L101-L104.

[75] Draine, B. T.; Lee, H. M., "Optical properties of interstellar graphite and silicate grains", ApJ 285 (1984) 89-108.

[76] Miyake, K.; Nakagawa, Y., "Effects of particle size distribution on opacity curves of protoplanetary disks around T Tauri stars", Icarus 106 (1993) 20-41.

[77] Hartmann, L.; Kenyon, S. J.; Calvet, N., "The excess infrared emission of Herbig Ae/Be stars - Disks or envelopes?", APJ 407 (1993) 219-231.

[78] Dullemond, C. P., Dominik, C., & Natta, A., "Passive Irradiated Circumstellar Disks with an Inner Hole" ApJ 560 (2001) 957-969

[79] D'Alessio, P.; Calvet, N.; Hartmann, L., "The Structure and Emission of Accretion Disks Irradiated by Infalling Envelopes", ApJ 474 (1997) 397-406

[80] Konigl, A.; Pudritz, R. E., "Disk Winds and the Accretion-Outflow Connection", Protostars and Planets IV, Tucson: University of Arizona Press; eds Mannings, V., Boss, A.P., Russell, S., (2000) 759.

[81] Calvet, N. "Properties of Winds of T Tauri stars", Proc. of IAU Symp. 182, eds. B. Reipurth & C. Bertout, Kluwer, (1997) 417-432.

[82] Petrov, P. P.; Herbig, G. H., "On the interpretation of the spectrum of FU Orionis", ApJ 392 (1992) 209-217.

[83] Calvet, N.; Hartmann, L.; Kenyon, S. J., "Mass loss from pre-main-sequence accretion disks. I - The accelerating wind of FU Orionis", ApJ 402 (1993) 623-634.

[84] Croswell, K.; Hartmann, L.; Avrett, E. H, "Mass loss from FU Orionis objects", ApJ 312 (1987) 227-242.

[85] Bouvier, J.; Cabrit, S.; Fernandez, M.; Martin, E. L.; Matthews, J. M., "Coyotes-I - the Photometric Variability and Rotational Evolution of T-Tauri Stars", AA 176 (1993)

[86] Eiroa, C.; Oudmaijer, R. D.; Davies, J. K.; de Winter, D.; Garzon, F.; Palacios, J.; Alberdi, A.; Ferlet, R.; C. A.; Cameron, A.; Deeg, H. J.; Harris, A. W.; Horne, K.; Merin, B.; Miranda, L. F.; Montesinos, B.; Mora, A.; Penny, A.; Quirrenbach, A.; Rauer, H.; Schneider, J.; Solano, E.; Tsapras, Y.; Wesselius, P. R., "On the simultaneous optical and near-infrared variability of pre-main sequence stars", AA 384 (2002) 1038-1049.

[87] Herbst, W., " The Rotation and Variability of T Tauri Stars: Results of Two Decades of Monitoring at Van Vleck Observatory", in Small Telescope Astronomy on Global Scales, ASP Conference Series Vol. 246, IAU Colloquium 183, edited by B. Paczynski, W.-P. Chen, and C. Lemme. San Francisco: Astronomical Society of the Pacific (2001) 177.

[88] Calvet, N.; Hartmann, L.; Hewett, R.; Valenti, J. A.; Basri, G.; Walter, F., "C IV in classical T Tauri stars", Cool stars; stellar systems; and the sun : 9 : Astronomical Society of the Pacific Conference Series, 109 (1996) 419.

[89] Bouvier, J.; Chelli, A.; Allain, S.; Carrasco, L.; Costero, R.; Cruz-Gonzalez, I.; Dougados, C.; Fernandez, M.; Martin, E. L.; Menard, F.; Mennessier, C.; Mujica, R.; Recillas, E.; Salas, L.; Schmidt, G.; Wichmann, R., "Magnetospheric accretion onto the T Tauri star AA Tauri. I. Constraints from multisite spectrophotometric monitoring", AA 349 (1999) 619-635.

[90] Terquem, C.; Bertout, C., "Tidally induced WARPS in T Tauri discs - II. A parametric study of spectral energy distributions", MNRAS 279 (1996) 415-428.